Bodei and colleagues review current understanding of receptor-guided tumor targeting with radionuclides and introduce an article in this month's *JNM* that offers new data for clinical applications in radionuclide therapy. . . . . ***Page 375***

Lindner and colleagues use ^{11}C-acetate PET to evaluate the effects of cardiac resynchronization therapy on myocardial oxygen consumption and cardiac efficiency in patients with severe heart failure and left bundle-branch block. . . . . ***Page 378***

Van Laere and colleagues investigate whether combined perfusion and dopamine transporter imaging can aid in early-stage differential diagnosis of parkinsonian disorders, including idiopathic Parkinson's disease, progressive supranuclear palsy, multiple system atrophy, dementia with Lewy bodies, and essential tremor. . . . . ***Page 384***

Pöpperl and colleagues compare extended analyses of ^{18}F-FET uptake kinetics with standard tumor-to-background ratios in PET prediction of tumor grade in patients with pretreated gliomas. . . . . ***Page 393***

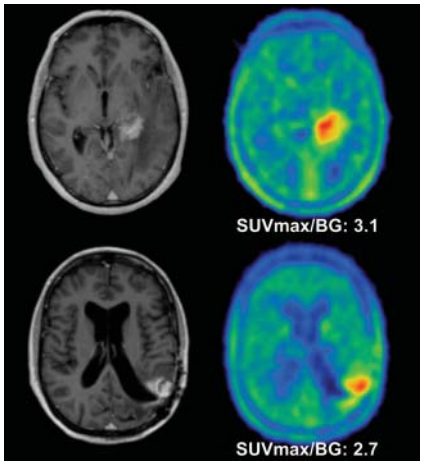

Kato and colleagues assess the relative usefulness of ^{123}I-IMP SPECT and ^{18}F-FDG PET for the detection of uveal malignant melanoma, the most common primary intraocular neoplasm in adults. . . . . ***Page 404***

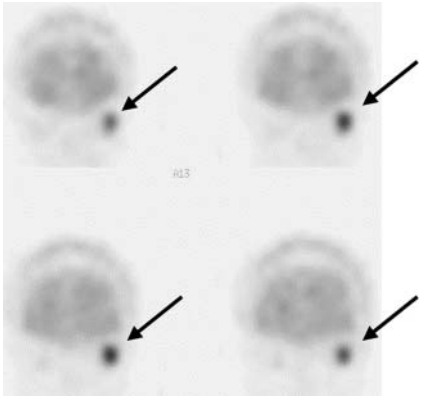

Cher and colleagues use ^{18}F-FMISO PET to assess hypoxia in newly diagnosed primary brain tumors and discuss its potential for directing patients toward targeted hypoxic therapies and monitoring treatment response. . . . . ***Page 410***

Guo and colleagues detail correlations between ^{18}F-FDG uptake on PET and microvessel density determined with different endothelial cell antibodies in lung adenocarcinomas and describe the prognostic implications of these findings. . . . . ***Page 419***

Hashimoto and colleagues examine the characteristics of solid pulmonary nodules with low ^{18}F-FDG uptake values and report on the ability of ^{18}F-FDG PET to differentiate benign from malignant lung diseases both visually and semiquantitatively. . . . . ***Page 426***

Vegt and colleagues research the effects of infusion of low doses of the plasma expander succinylated gelatin on renal uptake of ^{111}In-labeled octreotide and discuss possible toxicity-limiting applications in peptide receptor–mediated radiotherapy. . . . . ***Page 432***

Lee and colleagues characterize the mechanisms that mediate ^{123}I-MIBG transport in pulmonary endothelial cells and investigate the effects of stimuli associated with pulmonary dysfunction. . . . . ***Page 437***

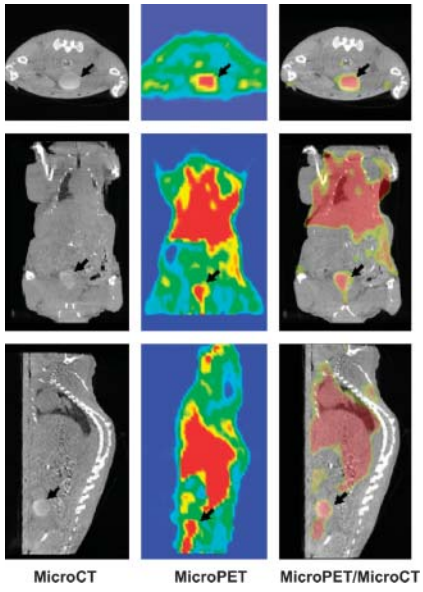

Yi and colleagues compare the diagnostic accuracies of helical dynamic CT and integrated PET/CT in patients with malignant solitary pulmonary nodules. . . ***Page 443***

Bunyaviroch and Coleman provide a comprehensive educational overview of the current practice and utility of PET in lung cancer. . . . . ***Page 451***

Brechtel and colleagues evaluate image coregistration results with 4 PET/CT examination protocols using contrast-enhanced single-phase or contrast-enhanced multiphase CT scans under different breathing conditions. . . . . ***Page 470***

Herrero and colleagues assess the relative abilities of ^{15}O-water and ^{11}C-acetate microPET in noninvasively quantifying myocardial blood flow in rats. . . . . ***Page 477***

Shichinohe and colleagues elucidate the mechanism of restored neurologic function through bone marrow stromal cell expression of the neuron-specific γ-aminobutyric acid receptor transplanted into a mouse model of cerebral infarction. . . ***Page 486***

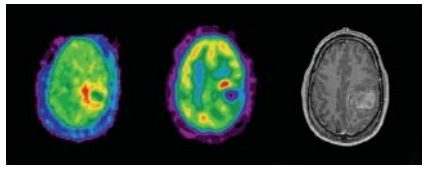

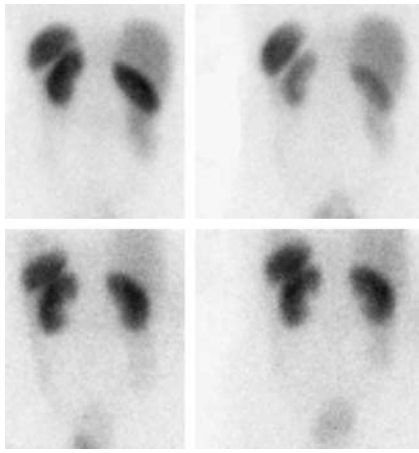

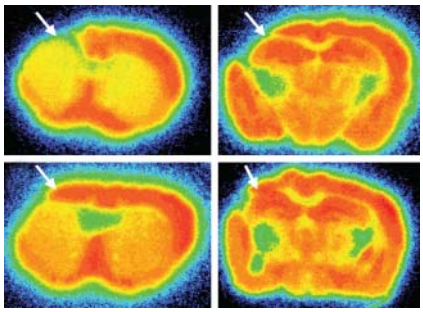

Orlova and colleagues prepare the ^{99m}Tc-labeled affibody dimer His_6-$(Z_{HER2:4})_2$, assess its targeting properties in vitro and in vivo, and discuss possible applications in imaging of HER2 expression in primary breast carcinomas and extrahepatic metastases. . . . . ***Page 512***

Zhang and colleagues describe the development of ^{18}F-labeled bombesin analogs for PET imaging of gastrin-releasing peptide receptor expression in prostate cancer xenograft models. . . . . ***Page 492***

Zoghbi and colleagues describe a radiometabolite generated by ^{18}F-FECNT, a PET radioligand for dopamine transporters, and investigate whether this radiometabolite may contribute to errors in PET imaging in human and nonhuman primate brains. . . . . ***Page 520***

Breitz and colleagues evaluate the pharmacokinetics and radiation-absorbed dose to all organs from the β-emitting radiopharmaceutical ^{166}Ho-DOTMP, which localizes to bone surfaces and shows promise for skeleton-targeted radiotherapy in multiple myeloma. . . . . ***Page 534***

Cescato and colleagues apply novel immunocytochemical methods to measure somatostatin receptor internalization induced by a variety of somatostatin analogs, facilitating characterization of trafficking of somatostatin receptor subtypes in vitro at the protein level. . . . . ***Page 502***

van Eerd and colleagues analyze the effects of several plasma expanders on the renal uptake of ^{111}In-octreotide in rats and mice and discuss the potential for limiting toxicity in radiolabeled peptide therapy. . . . . ***Page 528***

Schmidt and colleagues explore the antiangiogenic effects of human angiostatin gene transfer on tumor growth and changes in perfusion or blood volume, using in vivo measurements with PET, immunohistochemistry, and gene expression analysis. . . . . ***Page 543***

ON THE COVER

PET/CT protocols for single-phase (top) and multiphase (bottom) examinations. At top, the purple spiral represents the whole body in portal-venous contrast enhancement. The scan includes the base of the skull to the proximal thigh, as in PET (blue cylinder). At bottom, the technical standard of the multiphase protocol requires 2 CT examinations: one covering the base of the skull to the lower borders of the kidneys during arterial contrast enhancement (red spiral) and another covering the base of the lungs to the proximal thighs in portal-venous phase enhancement (purple spiral). After reconstruction, low-dose CT (gray spiral) and PET are performed. The thickness of the spirals indicates the dose, and the width the collimation.

SEE PAGE 472